MODEL DRIVEN ANALYSIS OF OPTICAL REFLECTANCE SPECTROSCOPY FOR DETECTION OF HUMAN PROSTATE AND KIDNEY CANCERS

By

ADITYA VIVEK MATHKER

Presented to the Faculty of the Graduate School of

The University of Texas at Arlington in Partial Fulfillment

of the Requirements

for the Degree of

MASTER OF SCIENCE IN BIOENGINEERING

THE UNIVERSITY OF TEXAS AT ARLINGTON

AUGUST 2008

ACKNOWLEDGEMENTS

I believe that research is always a group effort and would like to take this valued occasion to thank all my colleagues, collaborators & professors who laid the foundation for my research and never endingly helped me during my work.

A heartfelt and sincere thank you to my mentor Dr. Hanli Liu, who entrusted confidence in my naïve capabilities and gave me an opportunity to exhibit and develop my research skills under her preeminent guidance.

My inestimable gratefulness to my Parents, my Brother and God for their constant encouragement even in failure, their love when there was none, their trust in my potential and the help when I needed the most. A heartfelt condolence and thank you to my late cousin who will always remain one of my icons.

I would also like to thank Dr. Jeffrey Caddedu for giving us the invaluable specimens, Dr.Wareef Kabbani for histological analysis, Dr. Karim Bensalah and Dr.Altug Tuncel for assisting us in acquiring the data and also for their important novel inputs. My thanks also goes out to Dr. George Alexandrakis for teaching me the valued fundamentals of optics during his coursework and also for accepting my request to be a committee member.

Lastly a very special thank you to Disha Peswani, Sweta Narvenkar, Dheerendra Kashyap & Vikrant Sharma for their research support and encouragement during my thesis.

June 20, 2003

ABSTRACT

MODEL DRIVEN ANALYSIS OF OPTICAL REFLECTANCE SPECTROSCOPY
FOR DETECTION OF HUMAN PROSTATE
AND KIDNEY CANCERS

Aditya Vivek Mathker, M.S.

The University of Texas at Arlington

and

The University of Texas Southwestern Medical Center at Dallas, 2008

Supervising Professor: Dr. Hanli Liu

Renal cell carcinoma is one of the most common forms of kidney cancer originating from the renal tubule. During surgery, it is difficult for the surgeons to identify the cancer tissue from the normal tissue and also the benign tumor from malignant tumor. Moreover, prostate cancer is the leading cause of death amongst men in the United States. In this study, optical reflectance spectroscopy with short source-detector separation is used as a minimally invasive technique to differentiate normal tissues from tumor lesions and also to differentiate benign from malignant tissues in renal cell carcinoma.

Clinical post-operative readings were obtained using the optical spectroscopic equipment. 23 cases of prostate cancer and 20 cases of kidney cancer were investigated to derive statistical differences. An analytical model, reported by Zonios and Dimou, provides a

relationship, associating the measured reflectance with the reduced scattering coefficient ($\mu s'$) and hemoglobin concentrations of the measured specimens. The model is fitted optimally to the experimental data in order to quantify respective parameters of the human renal and prostate tissues.

After analyzing the clinical data, we obtained statistical differences in the oxy-hemoglobin (HbO) and deoxy-hemoglobin concentrations (Hb). The Student t-test was performed to show that p-values of 0.03 and 0.04 were obtained for the HbO and Hb components, respectively, while comparing the benign and malignant renal cell carcinomas. A significant differentiation was also observed between normal and cancerous tissues measured from the outside of the kidney [p-value = 0.04 (HbO), 1.36E-07 (Hb) & 0.03 (μ_s')]. For the prostate, the statistical difference between the readings taken on the normal and cancerous tissue was significant with a p-value of 0.02 for HbO, 0.03 for Hb and 4.07E-06 for μ_s'. These results have illustrated the feasibility of optical spectroscopy to be a viable technique for clinical detection of cancer.

TABLE OF CONTENTS

LIST OF ILLUSTRATIONS

LIST OF TABLES

CHAPTER 1

INTRODUCTION

1.1 Prostate

Prostate is a small walnut sized exocrine gland of the male reproductive system. It is located in the pelvis, below the bladder, in front of the rectum and above the sphincter & the penis. The ducts of the prostate are lined by transitional epithelium. The main function of the prostate is that it make's a slightly alkaline fluid which constitutes about 10-30% of the seminal fluid. This fluid along with the spermatozoa makes up the semen [1]. This fluid activates the sperms during ejaculation. The alkalinity of the liquid neutralizes the acidity of the vaginal tract thus prolonging the lifespan of the sperm. The urethra passing through the center of the prostate and merges with the ejaculatory ducts (the male urethra has two functions). The gland is enclosed on the pelvic floor muscles which contract during ejaculation. The prostate can be divided into four distinct zones pathologically [4, 5].

1. Peripheral Zone: It is the sub-capsular portion of the gland surrounding the urethra. There is 70% chance for the origin of cancer from this zone.

2. Central Zone (CZ): It surrounds the ejaculatory ducts. This zone constitutes to about 25% of the prostate cancer origin.

3. Transition Zone (TZ): This region is responsible for benign prostatic hypertrophy. There is a mere 5% chance for the origin of cancer from this zone.

4. Anterior fibro-muscular Zone: It is made up of the muscles and the fibrous tissue.

1.1.1 Digital Rectal Examination (DRE)

It is a medical exam in which a physician or a health professional palpates the prostate. The procedure is performed to check for cancer growth or enlargement of the prostate structure.

During the examination, the physician or the professional puts a lubricated gloved finger of one hand into the rectum. Prostate cancer feels like a hard lump during the procedure. The physician presses firmly on the prostate to feel for any problems. This pressure might lead to the urge to urinate as the urethra passes through the prostate. Abnormal surface of the prostate could mean the presence of benign prostatic hypertrophy (BPH) or prostatitis [7].

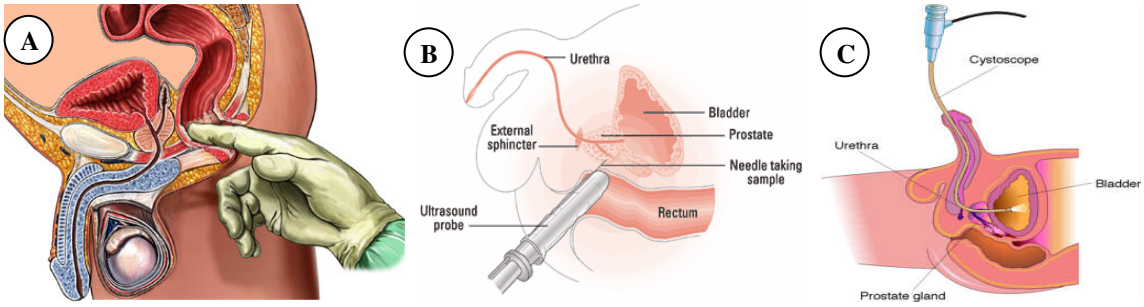

Figure 1.1 Procedures for Prostate Cancer Diagnosis. (A) Digital Rectal Examination. (B) Trans-rectal Ultrasound & (C) Cystoscope [14].

1.1.2 Trans Rectal Ultrasound (TRUS) & Biopsy

This procedure is performed when the results of a DRE or PSA are abnormal. Trans Rectal Ultrasound involves a small probe which is inserted through the rectum. The high frequency ultrasound waves bounce off the surface of the prostate. The receive signals are then transformed into a real time video. The probe can capture images are different angles and locations. Usually the probe is used to guide the surgeon to select the appropriate location for inserting the biopsy needles. The probe has a small insertion through which the needle is inserted [8]. Usually six or more biopsies are taken from various parts of the prostate. The

needle quickly enters the gland and takes out the samples. The tissue samples are then analyzed for the presence of cancer cells. The pathologist assigns a grade (Gleason score) which will indicate the presence and the aggressiveness of the cancer cells. Other than the rectum, ultrasound biopsies can be conducted through the urethra or the perineum. In transurethral biopsy a cystoscope is inserted into the urethra. This allows the physician to examine the prostate gland and then by passing a cutting loop through the scope the tissue samples are taken out. A perineum biopsy involves making a small incision in the perineum. The physician then inserts a finger into the rectum and subsequently inserts a needle to collect the sample.

1.1.3 Prostate Specific Antigen (PSA)

PSA is a protein produced by the prostate cells. In a PSA test the doctor takes a blood sample from the patient and the amount of PSA content is measured by pathology. PSA is also known as the Prostate marker. The amount of PSA content cannot be established as the signs of benign conditions or cancer. PSA levels are generally low in men but they vary due to age, hormonal conditions, prostatitis, Benign Prostatic Hyperplasia (BPH) or cancer [9, 11]. The test results are measured as nanograms of PSA per milliliter (ng/mL) in the given sample of blood. Earlier, the occurrence of prostate was usual in men having PSA greater than 4.0ng/mL, but recent studies have reported men with PSA less than 4.0ng/mL with prostate cancer. (2) Currently the following ranges of PSA levels are considered for occurrence of prostate cancer:

- 0 to 2.5ng/mL is low.
- 2.6 to 10ng/mL is slightly to moderately elevated.
- 10 to 19.9ng/mL is moderately elevated.

- 20.0ng/mL or more is significantly elevated.

There is no fixed level of PSA for cancer, but as the PSA level increases the likelihood of cancer is higher. Doctors normally do not recommend additional treatment based on only the PSA results. Rather, the trend of PSA levels over a period of in conjunction with other findings like abnormal DRE, positive prostate biopsy results, or abnormal CT are used to decide the further course of treatment. According to National Comprehensive Cancer Network (NCCN) Clinical Practice Guidelines in Oncology for Prostate Cancer (3) the following categories of patient's mite require additional treatment:

- PSA levels have doubled in the last 3 years.
- PSA velocity (change in PSA levels over time) is greater than 0.75ng/mL.
- PSA levels do not become negligible or if the PSA levels are higher that 0.3ng/mL for patients who have undergone radical prostatectomy (removal of the prostate gland)

The reasons why PSA level is not considered as the principle marker for onset of prostate cancer are:

- False positive tests: Around 25 to 30 percent of cases are false positives. It means that, though the level of PSA was high there were no signs of cancer (4).
- False negative tests: In this case the PSA levels are in the normal range but still cancer is present.

To overcome these inadequacies of PSA tests, new methods are being researched to make the PSA a viable tool for cancer detection. Some of the new techniques being evolved are as follows:

- PSA velocity: It is defined as the change in the PSA levels over a period of time. Studies have found that a 0.35ng/mL rise in the levels per year could be attributed to very high risk of prostate cancer compared to a change less than 0.35ng/mL(5).

- Age-adjusted PSA: In this norm of classification, different PSA levels are categorized for different age groups (10 year age group). Example, a PSA less than 2.4ng/mL for a 50 year old can be considered normal whereas PSA levels up to 6.5ng/mL could be considered normal for patients over 70 years of age.

- PSA density: It is a ratio between the PSA level and the size of the prostate. If a person has a larger prostate then PSA content will be higher compared to a person having a relatively smaller prostate. The drawback of this technique is that, at times the cancer could be overlooked for person having a large prostate.

- Free versus attached PSA: PSA is mainly present in two forms; attached to a protein molecule and free PSA. Free PSA levels help to tell what kind of prostate problem a patient has. BPH resembles high number of free PSA whereas cancer produces more PSA in the attached form. So, if a patient has high PSA, but his free PSA level is less, then the presence of cancer is very likely.

- Modification of PSA cutoff level: Researchers have recommended the lowering of the PSA levels for normal to about 2.5 or 3.0ng/mL from the current 4.0ng/mL. The drawback of

this could be that, this would increase the rate of false positives but inversely it would also lead to increased chances of prostate cancer detection [12, 13].

1.2 Kidney

The kidneys are located on the posterior part of the abdomen on the either side of the spine. The right kidney sits below the liver whereas the left below the diaphragm. The upper parts of the kidney are partially protected by the 11th and 12th rib, and it is surrounded by two layers of fat viz. perirenal and pararenal fat. The main functions of the kidney are excretion of waste products, homeostasis, acid-base balance, blood pressure regulation, plasma volume and hormone secretion.

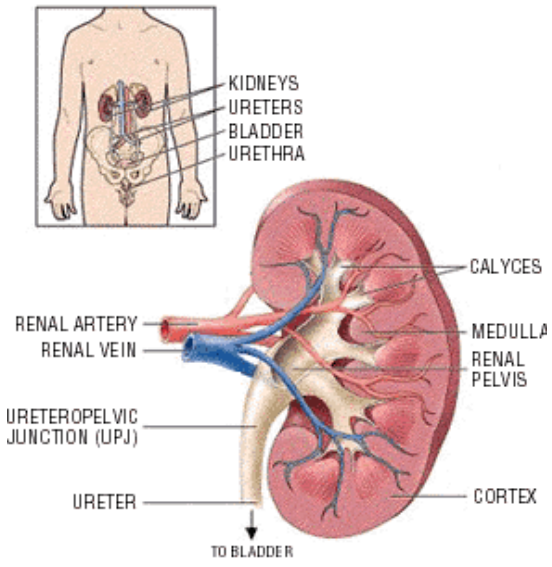

Figure 1.2: Anatomical location of the kidney in the body (inset) and the sectional area of the kidney [15].

The basic functional unit of the kidney is the nephron. The main function of the nephron is to regulate the concentration of water and salts by filtering the blood. Another main role of the nephron is reabsorbing the require salts and constituents and excreting the rest as urine from the body. The working of the nephron is regulated by the following hormones: antidiuretic hormone, aldosterone, and parathyroid hormone.

As per the latest statistics published by the National Cancer Institute, there were estimated 54,390 cases of kidney caner in 2008 and almost 85% of them were renal cell carcinomas. Almost one in three patients dies due to kidney cancer. This is relatively a very high mortality rate. There are majorly two types of surgeries done to treat kidney cancer viz. Radical Nephrectomy and Partial Nephrectomy [2].

1.2.1 Radical Nephrectomy

In this surgery, the entire kidney has to be removed due to the excessive spread of the tumor. During the removal, along with the kidney, the adrenal gland and some of the lymph nodes are also removed.

1.2.2 Partial Nephrectomy

It is a nephron-sparing procedure in which the tumor is removed while keeping the non-cancerous part of the kidney intact. The type of surgery generally occurs in the early stages of the cancer, mostly in stage 1 cancer.

CHAPTER 2

INSTRUMENTATION

The instruments used for acquiring the spectrums from the specimens consisted of the spectrometer (USB 2000, Ocean Optics Inc., Dunedin, FL), a tungsten-halogen light source, a laptop with Lab view interface software and a fiber optic linear array probe [10]. The spectrometer had a wavelength acquiring range of 400nm – 1100nm. Figure 2.1 illustrates the internal working mechanism of the spectrometer.

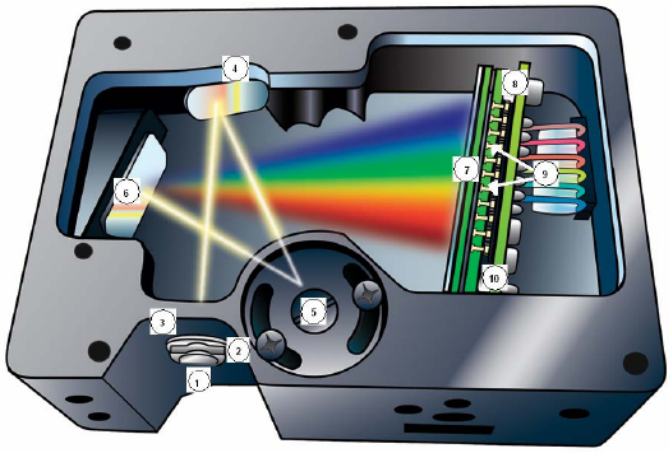

Figure 2.1: The figure shows the internal working mechanism of the USB 2000 spectrometer [10].

Label 1 depicts the SMA 905 through which the light enters the optical bench. The amount of light and wavelength which enters the spectrometer is regulated by the Slit (2) and

the Filter (3). SAG+, Ag-coated collimating mirror (4) focuses the selected wavelength regions onto the grating (5). The light is received by the focusing mirror (6) which in turn reflects the light onto the L2 Detector Lens (7). The Detector (8) then converts the optical light into a digital signal. Every pixel on the CCD array detector responds to the respective wavelength of light that strikes it and transmits the response to the software application.

A halogen High Power Light Source (HL-2000-HP, Ocean Optics Inc., Dunedin, FL) with a wavelength range of 360nm to 2000nm was used. The probe used for acquiring the data was a 7 linear array bi-furcated optical probe. 7 separate pairs of source-detectors were used as shown in figure 2.2 (C). The separation between each pair was about 100µm. For the experiment fiber 3 was used as the source fiber and fiber 5 was used as the detector fiber. The approximate separation between fiber 3 & fiber 5 was 300µm. These two fibers were selected due to the proximity to the center of the array probe, eases the use of the probe. The schematic of the probe is depicted in figure 2.2(C). The spectra obtained were all reference to a reflectance calibration standard (WS-1, Ocean Optics, Dunedin, FL). The software program used for the acquiring the spectrums was designed using Lab View interface software (National Instruments, Austin, TX).

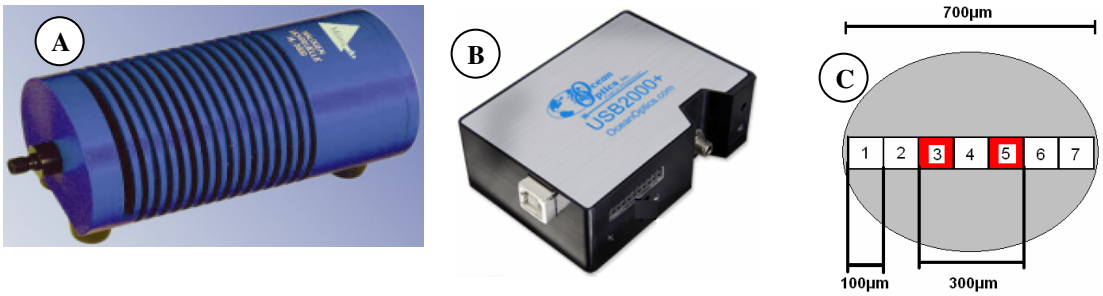

Figure 2.2: (A) The halogen light source. (B) The USB 200 Spectrometer (C) The cross-sectional geometry of the probe tip. The number 1-7 depict the different source-detector fibers. In the above experiment, "3" was used as the source and "5" as the detector.

The linear array fiber was placed on the kidney and the prostate samples and the reflectance spectra were obtained. The first reading was the background reading which was obtained by switching off the room lights and the light source. The probe was placed on the sample in the dark and the reading was obtained. We shall study the impact of the background subtraction in the following chapter. In the next step, the readings were obtained from the sample was the reference schematic maps which were prepared by the surgeons. These maps exhibited the approximate locations on which the readings should be taken. The figures

exhibited in Chapter 4 show the maps for Partial Nephrectomy, Radical Nephrectomy and Prostatectomy.

The probe was then placed on the respective locations and the spectrums were obtained. The effects from the fiber, light source and the spectrometer were removed by dividing the obtained spectrum by the similar spectrum obtained from the reference sample (white sample) [3]. The sample provided ~100% reflectance in the wavelength length of our interest (Diffuse Reflectance Standard Specifications, Ocean Optics, FL).

CHAPTER 3

REFLECTANCE MODEL

Reflectance spectroscopy is being increasing used to for tissue characterization and classification. Quantification of spectrums acquired from the tissues is highly desirable as it is a minimally invasive technique. Diffusion approximation of has been widely researched to study the light propagation in the Biological tissues. It is necessary to develop computational techniques to enumerate the physiologically correlative components of the tissues for detection and differentiation of biological samples. The inadequacy of the diffusion approximation is the requirement of stringent boundary condition for its application: (1) the source-detector separation must be greater than the transport mean free path distance and (2) the reduced scattering coefficient, μ_s' must be greater than the absorption coefficient, μ_a. The reduced scattering coefficient μ_s' can be defined as the mean distance travelled by the photon before it gets scattered (absorbed) [19]. μ_s' is dependent on two variable viz. μ_s and g [6]. Their correlation is as follows:

$$\mu_s' = \mu_s (1-g)$$

Where μs is the cross-sectional area per unit volume of medium and g is the amount of forward direction retained by the photon after a single scattering event. The major chromospheres which absorb light in the visible region (380 – 780nm) are oxygenated and deoxygenated hemoglobin (HbO and Hb respectively).

In our study we could not implement the diffusion reflectance approximation models as the source – detector separations were small. At separations < 1mm and by virtue of using the visible light, the absorption coefficient becomes comparable to the reduced scattering coefficient. Due to this the diffusion theory fails. The method developed by our group is

promising for real time quantification of blood parameters dynamically. This technique is easy to implement, universal in application and sturdy. The procedure is semi-empirical in conjunction with the ant colony optimization model for the quantification of the hemoglobin parameters along with the scattering coefficients. The analytical model is based on the recent publication by Zonios and Dimou. The implementation of the model was basically done in three steps:

1. Rigorous calibration of model parameters k1 & k2.
2. Development of ant colony optimization model for calculating the reduced light scattering coefficient and the hemoglobin concentrations [18].
3. Implementation of this model to analyze Prostate and Kidney Cancer tissues.

3.1 Calibration of k1 & k2

The semi – empirical model developed by Zonios and Dimou relates the reflectance, reduced scattering coefficient and the absorption coefficient as follows:

$$R_p(\lambda) = \frac{1}{k_1 \frac{1}{\mu's(\lambda)} + k_2 \frac{\mu_a(\lambda)}{\mu_s'(\lambda)}}$$

Where Rp is the reflectance measurement at λ, μ_a is the absorption coefficient at λ and μ_s' is the reduced scattering coefficient. k_1 & k_2 are the calibration parameters which depend upon the characteristics of the probe and the hardware components assigned to the respective measurements. μ_a is a function of the Hb, HbO, melanin concentration and water concentration as given below:

$$\mu_a(\lambda) = [HbO]\,\varepsilon_{HbO}(\lambda) + [Hb]\,\varepsilon_{Hb}(\lambda) + [H_2O]\,\varepsilon_{H_2O} + [C_{mel}]\,\varepsilon_{mel}(\lambda)$$

where ε_{HbO}, $\varepsilon_{Hb}(\lambda)$, ε_{H_2O}, $\varepsilon_{mel}(\lambda)$ are the extinction coefficients for HbO, Hb, water and melanin respectively.

The μ_s' is derived using the following relationship:

$$\mu_s'(\lambda) = \left(1 - \frac{d_o^{1/2}}{d_s^{1/2}} \frac{\lambda - \lambda_{\min}}{\lambda_{\max} - \lambda_{\min}}\right) \mu_s'(\lambda_{\min})$$

Where λ_{max} = 900nm and λ_{min} = 500nm. d_s represents the effective scatter size and d_o is the published constant and its value is 0.0625μm. The μ_s' is an equivalent approximation of the Mie theory of scattering based on the publication by Flock et al [20]. As observed from the above equation, the maximum and minimum λ have been considered in accordance with the visible and the near infrared window of the light spectrum.

3.2 Calculation of Absorption and Scattering Coefficients

The absorption coefficients were calculated from the measured concentrations and from the published extinction coefficients. For calculating the μ_s' we used the scattering Mie theory model published by Staveren et al [21]. The published equation for calculating μ_s' for 10% of Intralipid solution is:

$$\mu_s = (2.54 \times 10^{9})(\lambda^{-2.4}) \ [cm^{-1}]$$

$$g = 1.1 - (0.58 \times 10^{-3})*(\lambda)$$

$$\mu_s' = \mu_s (1-g)$$

Thus using the above equations the reduced scattering coefficient is approximated. The above equation is for 10% of intralipid. For calculating the μ_s' range for respective calibration intralipid concentration is calculated as follows:

Assume the following for x% concentration of intralipid,

$$\mu_s' (750nm)_x = A$$

$$\mu_s' (830nm)_x = B$$

A & B are obtained from the ISS oximeter during the calibration process.

We know from the μ_s' equation, at 10% Intralipid, the values of μ_s' at 750nm & 830nm.

$$C = \frac{\mu_s'_{750nm}}{A}$$

$$D = \frac{\mu_s'_{830nm}}{B}$$

To calculate the μ_s' (λ) for x % Intralipid, we average the two ratios C & D. The product of the average of then used to divide the entire range of λ for 10% intralipid. Thus we can obtain the μ_s' at any given Intralipid solution.

3.3 Calculation of μ_a

The extinction coefficients for HbO and Hb are obtained from **Scott Prahl's** compilation. During the calibration process the extinction coefficients (μ_a) are obtained from the ISS Oximeter at 730nm and 850 nm. To calculate the Hb and HbO concentration from the values of μ_a the following equations were used:

$$HbO_2 = ((\mu_{a750}*\varepsilon_{Hb830})-(\mu_{a830}*\varepsilon_{Hb750})) / (\varepsilon_{HbO2\ 750}*\varepsilon_{Hb830} - \varepsilon_{HbO2\ 830}*\varepsilon_{Hb750})*1000;$$

$$Hb = -((\mu_{a750}*\varepsilon_{HbO2\ 830})-(\mu_{a830}*\varepsilon_{HbO2\ 750}))/(\varepsilon_{HbO2\ 750}*\varepsilon_{Hb830} - \varepsilon_{HbO2\ 830}*\varepsilon_{Hb750})*1000;$$

After obtaining the values, the range of μ_a for the respective wavelengths was found. The equation used to calculate the range of μ_a was:

$$\mu_a(\lambda) = [HbO_2] * \varepsilon_{HbO2}(\lambda) + [Hb] * \varepsilon_{Hb}(\lambda) + \varepsilon H_2O * \%H_2O$$

Thus using the above set of equations the entire range of the respective μ_a were calculated for the different blood concentrations.

3.4 Determination of k1 & k2

As mentioned earlier the empirical equation stated by Zonios and Dimou [17] can be re written as follows:

$$\frac{\mu_s'}{R_p} = k_1 + k_2\mu_a$$

From the calibration procedure and the calculations, we know the values of μ_s', R_p and μ_a.
The above equation is a resemblance of the equation of a linear line, which can be written as:

$$y = mx + c$$

Comparing the above two equations we can confer that:

$$y = \frac{\mu_s'}{R_p} \quad ; \quad m = k_2 \quad ; c = k_1$$

The above relations can be better understood by observing the following graph:

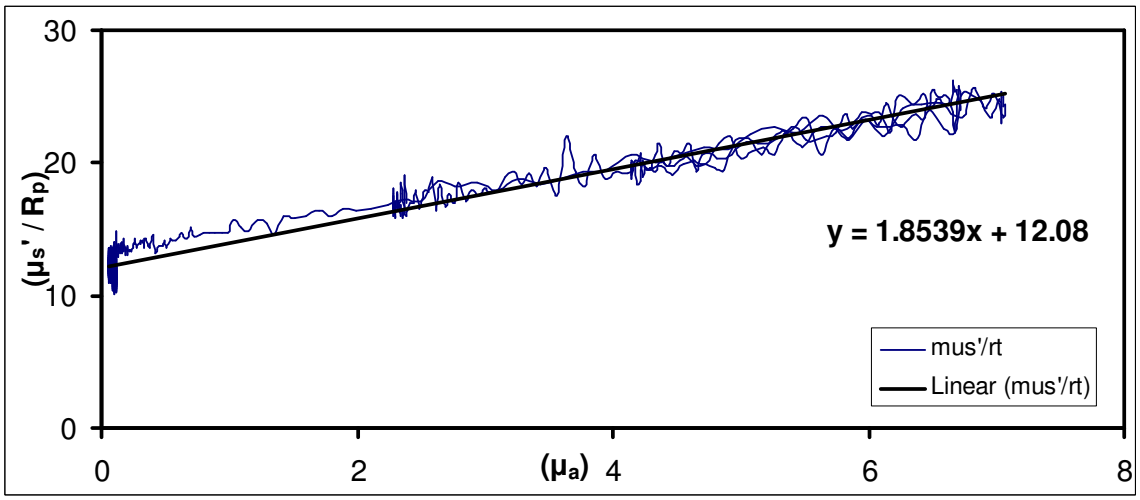

Figure 3.1: The above graph shows the calculation of k1 & k2. The linear fit equation resembles the equation of a straight line which is then comparable to the model equation to derive k1 & k2.

A graph is plotted with ($\frac{\mu_s'}{R_p}$) on the Y- axis and (μ_a) on the X-Axis. A linear fit is then implied to the graph and the equation is plotted. The Equation now resembles the k_1 and k_2 values.

3.5 Effect of Variation of k_1 and k_2 on Spectrum

To better understand the actual effect of k_1 and k_2 on the light spectrum, we applied the above equation to a sample data which was acquired from a 200μm separation optical fiber probe.

Intralipid Concentration	Hb_{Total} (µM)	Intergration Times (ms)	k_1	k_2
0.5%	15	50	11.74	4.51
0.5%	15	100	11.58	4.48
0.5%	25	50	10.97	4.35
0.5%	25	100	11.6	4.61
1%	15	50	9.82	3.59
1%	15	100	9.8	3.52
1%	25	50	10.68	4.05
1%	25	100	10.67	3.92
1.5%	15	50	11.45	5.29
1.5%	15	65	11.46	5.01
1.5%	25	50	11.63	4.84
1.5%	25	65	11.62	4.7
		Average	**11.085**	**4.406**
	Standard Deviation (Stdev)		**0.70**	**0.55**
	Percentage Stdev (%)		**6.32**	**12.42**

Table 3.1: The above table shows the intralipid calibration readings obtained from a 400µm separation probe at different concentrations.

As seen from the above graph, readings were taken at three different intralipid solutions. At each Intralipid concentration two 2 readings at two different total blood concentrations and respectively two different integration times were obtained. To calculate the Reflectance the empirical equation was re-written as follows:

$$R_p = \frac{\mu_s'}{k_1 + k_2 \mu_a}$$

where μ_s' was obtained from the Mie theory and μ_a was obtained from the human blood extinction coefficients. In the first figure, the value of k_1 is kept a constant (11.08) and the value of k_2 is varied as 3.86, 4.0, 4.40, 4.6 & 4.94. All these values are with the 12% deviation obtained for k_2.

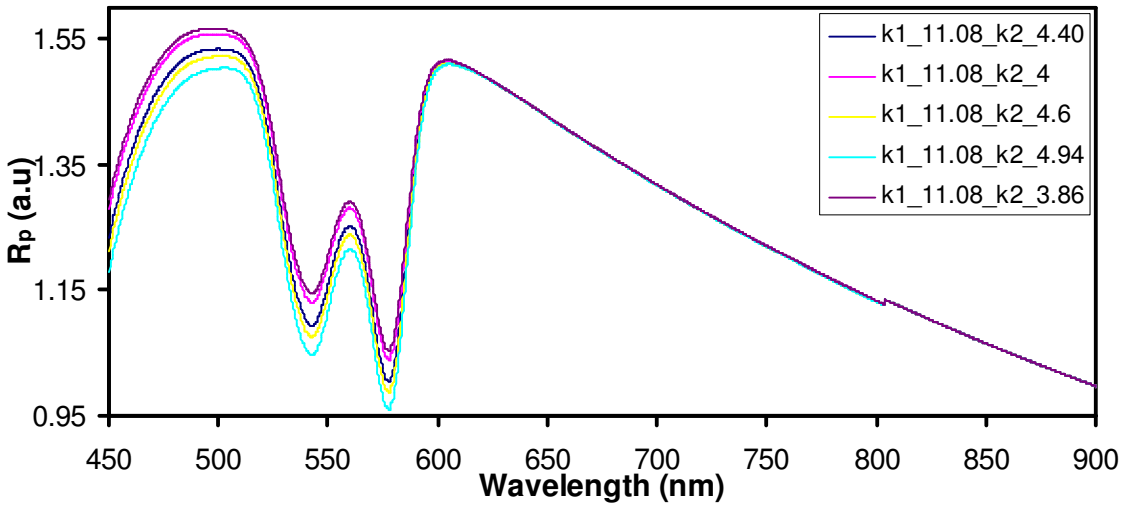

Figure 3.2: The above spectrum illustrates the variation of k2 when k1 is kept constant

In the second case, the value of k_2 was kept constant and the value of k_1 was varied within the limits of the obtained standard deviation. The values of k_1 were 11.08, 11.35, 10.60, 11.78 & 10.38.

As observed from both the above plots, the effect of variation of k_1 comparatively a larger impact on spectrum compared to the variation of k_2. The variation of k_2 affects majorly the visible range of the spectrum. This region corresponds to the wavelengths of blood absorption. This fact is quite evident from the equation, as we can observe that k_2 is multiplicative to μ_a. It has also been observed that the product of k_2 and μ_a is quite negligible compared to the value of k_1. Due to this μ_s' is less dependence on the value or variation in k_2. From the second plot, it can be noted that variation in k_1 not only affects the spectrum in the visible range but also the near infrared region. This fact gives us a better understanding of the behavior of k_1 and k_2.

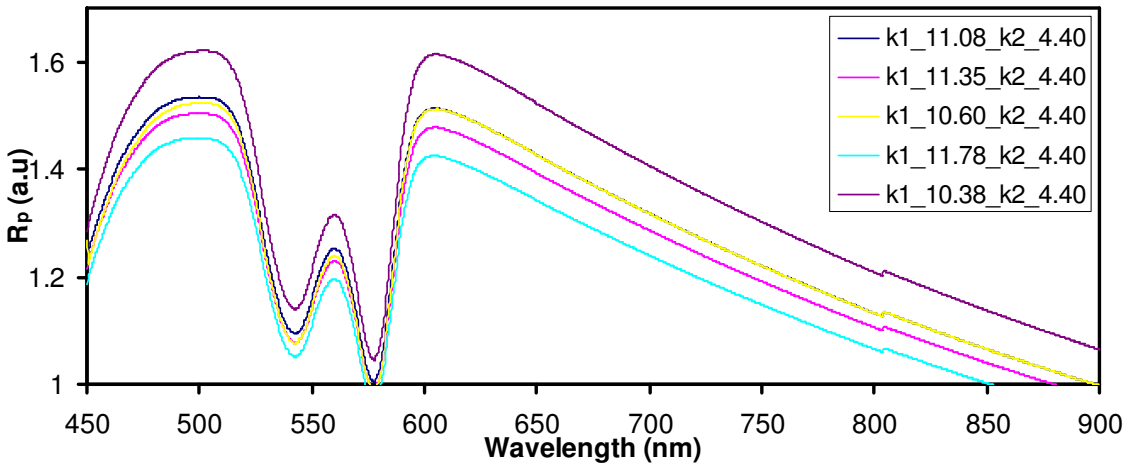

Figure 3.3: The above spectrum illustrates the variation of k1 when k2 is kept constant

3.6 Effect of Reduced Scattering Coefficient (μ_s') on k_1 and k_2

We have seen that from the empirical equation k_1 and k_2 are directly dependent on μ_s'. The study was conducted to quantify the exact changes which reflect on the values of k_1 and k_2 due to the scattering coefficient variation. The probe used was to study was the linear array probe which was explained in the earlier chapter. During calibration the data was obtained for different values of scattering coefficients at different integration times, but at constant blood concentration of 40μM. As the blood concentration was kept constant, any errors or variations which could occur while disturbing the hardware setup were ruled out. Otherwise, when the blood concentration needs to be modified, the ISS oximeter and the fiber optic probe have to be removed carefully and then retain the same setup one the new solution is prepared. This experiment also gives an understanding of the effect of probe movement between the calibration on the resultant values of k_1 and k_2.

	0.35 % I.L. (3.7mus)		0.5 % I.L. (5.8mus)		0.64% I.L. (7.1mus)		0.93% I.L. (10mus)		1.64% I.L. (16mus)	
Integration Time	k1	k2	k1	k2	k1	k2	k1	k2	k1	k2
200 ms	6.93	2.35	5.93	1.47	5.58	1.27	5.08	0.82	3.55	0.33
400ms	6.86	2.41	6	1.53	5.74	1.26	5.11	0.84	3.6	0.34
Average	**6.90**	**2.38**	**5.97**	**1.50**	**5.66**	**1.27**	**5.10**	**0.83**	**3.58**	**0.34**
Standard deviation	**0.05**	**0.04**	**0.05**	**0.04**	**0.11**	**0.01**	**0.02**	**0.01**	**0.04**	**0.01**
% Standard Deviation	**0.72**	**1.78**	**0.83**	**2.83**	**2.00**	**0.56**	**0.42**	**1.70**	**0.99**	**2.11**

Table 3.2: Variation of k1 and k2 for different I.L. concentrations for the linear array probe.

The above table shows the variation of k1 & k2 for the different concentrations of Intralipid Solutions. The experiment was carried out using a linear array probe with fiber 7 as the source and fiber 5 as the detector. As observed, the variation for a respective concentration of I.L. is much lesser. Thus, we could attribute the fact that the k1 & k2 are dependent on the μ_s' coefficient in the human tissue.

3.7 Effect of Background Light during Spectrum Processing

The raw spectrums obtained from the specimen need to be processed so that the effect of the background noise and the errors due to physical probe designs can be eliminated. The first step for processing the spectrum is to subtract the background light spectrum. This spectrum taken during the process of calibration with all the external room lights switched off. This subtracted spectrum is then divided by the respective spectrum obtained from the reference sample (white sample). Even the reference sample spectrum needs to be subtracted for background. The important criterion during the division by white sample is that, both the specimen and the reference spectrum need to be obtained at the same integration time. We shall study the effect of the reference spectrum in the next section. Let us sample two processed sample spectra, first one in which the division is done after background subtraction and the second one is which only the reference spectra is subtracted not the sample spectra.

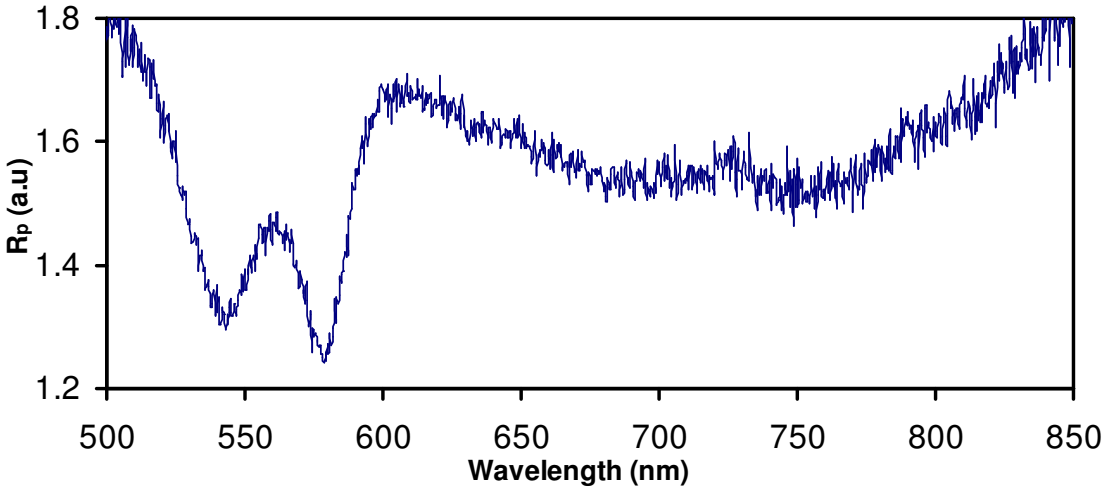

Figure 3.4: The above spectrum shows the processed spectrum when there was no background subtraction was done.

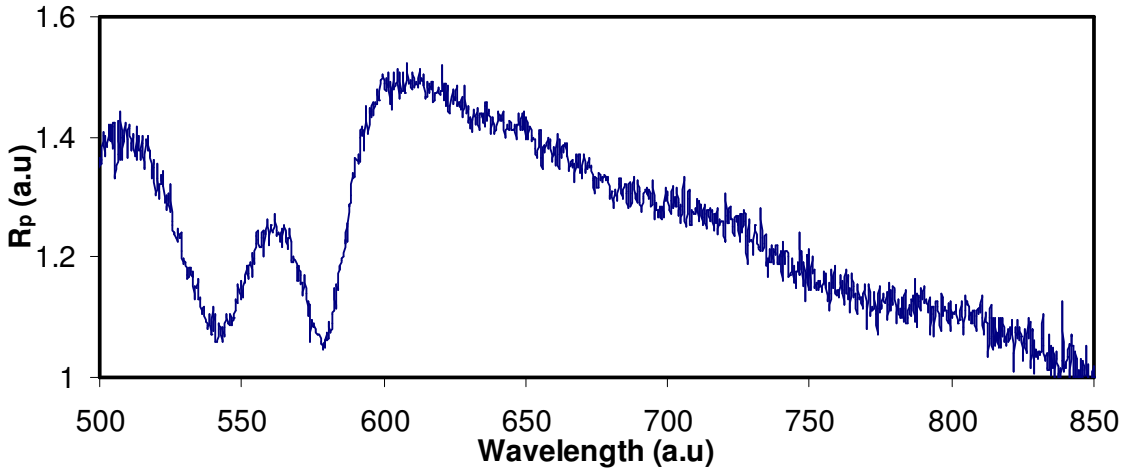

Figure 3.5: The plot resembles a processed spectrum after the background subtraction was done.

We can observe from the first plot that the pattern of reflectance after 600nm is not consistent. The usual pattern for the reflectance is shown in the second figure. The “U” pattern observed in the first plot is due to the background light. When the sample was acquired the background light was not subtracted. But the reference spectrum is without the background light. Let us plot the raw spectrum for both of them and observe the changes.

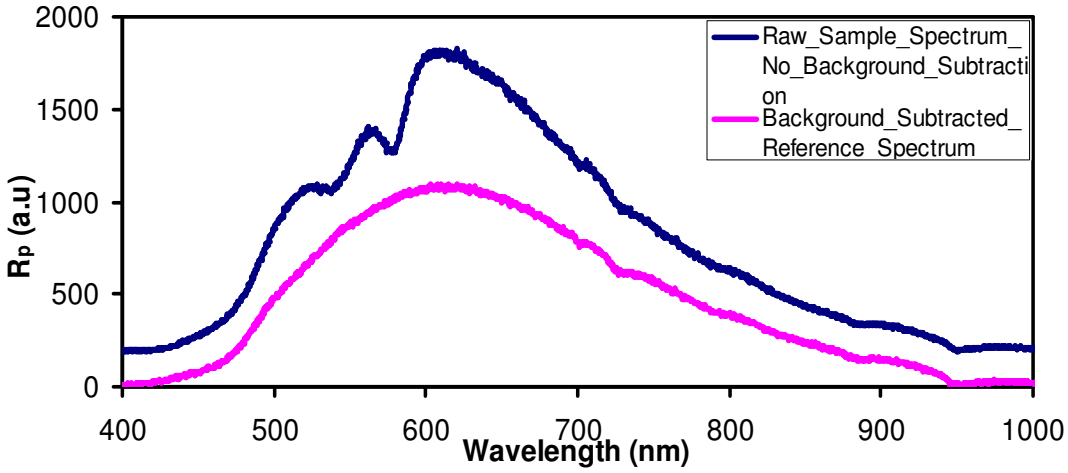

Figure 3.6: It can been observed that there is a background window between the raw sample and the reference sample spectrum. This window causes the “U” pattern of the processed spectrum.

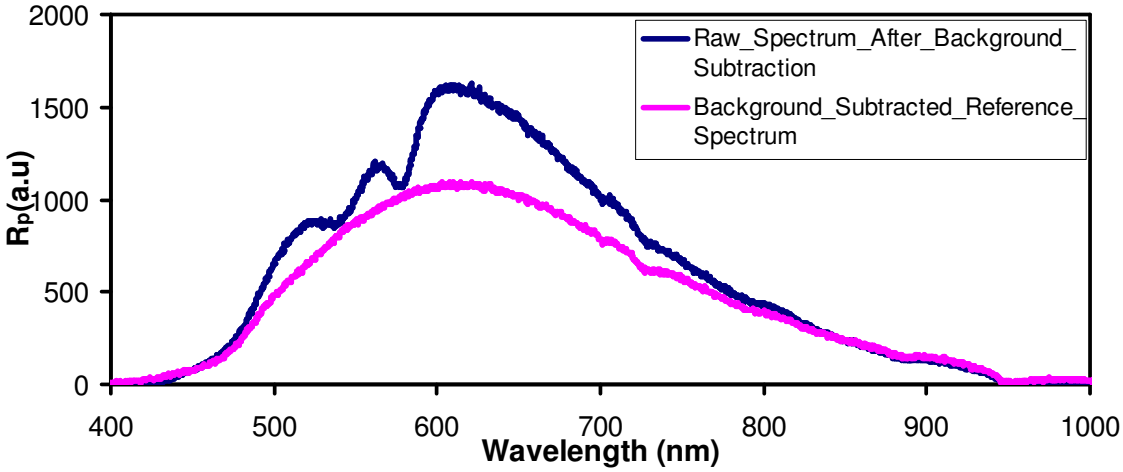

Figure 3.7: It can been observed that there is no background window between the raw sample and the reference sample spectrum. This will eliminate the “U” pattern.

Wavelength (nm)	Rp(a.u) [Sample] (A)	Rp(a.u) [Reference] (B)	Ratio [(A)/(B)]
550	1204	885.5	1.36
600	1786	1060.5	1.68
650	1635	1028	1.59
700	1220	779	1.57
750	855	579	1.48
800	626	388	1.61
850	436	236	1.85
900	338	144.5	2.34

Table 3.3: This table compares the ratio of the reflectance obtained at different wavelengths between raw data and the reference data.

In the first plot, there is a background window between the raw sample and the reference spectra. To analyze the behavior of the “U” pattern, let us tabulate a get data points from the region of that pattern at around 8 different wavelengths.

From the table it can be seen that, the “U” pattern is dependent on the ratio between the Sample and the reference. The Ratio decreases as the wavelength decreases till about 750nm and then it starts increasing, thus resembling “U” pattern.

Comparatively let us tabulate the same variables for a typical case.

Wavelength (nm)	Rp(a.u) [Sample] (A)	Rp(a.u) [Reference] (B)	Ratio [(A)/(B)]
550	1004	885.5	1.13
600	1586	1060.5	1.50
650	1435	1028	1.40
700	1020	779	1.31
750	655	579	1.13
800	426	388	1.10
850	236	236	1.00
900	138	144.5	0.96

Table 3.4: This table compares the ratio of the reflectance obtained at different wavelengths between raw data and the reference data after background subtraction.

The ratio in the above case decreases consistently from 600nm. Thus we can state that the background light has to be always subtracted before the spectrums are processed.

3.8 Optimization Theory

The algorithm implemented in our analysis is based on the technique of Ant colony optimization which was derived by Marco Dorigo et al. It is a probabilistic problem solving algorithm which is based on finding the short paths from the initialization to the end. This algorithm is developed from the theory of the movement of ants. Initially the ants wander around randomly to find food. Once they find food they return to their base colony while leaving a trail of pheromone. Thus this trail acts as a path to follow for the other ants. Over a period of time, this pheromone starts to evaporate. If the distance is short then the same path gets selected numerous times and thus the concentration of pheromone remains high. Thus the theory of creating the tail is a positive feedback mechanism which will be followed by all the ants. The advantage of pheromone trail is that, it prevents the creation of local minima. This avoids the solution space to be limited.

The mathematical model was formulated by Kashyap et al [22] and was implemented on our clinical data. The parameters for which the model fitting was done were oxy-hemoglobin concentration, de-oxy hemoglobin concentration and the scattering ratio.

CHAPTER 4

RESULTS

Readings were acquired from the kidney and prostate specimens after the patients had undergone laparoscopic nephrectomy and prostatectomy respectively. The data was acquired at the University of Southwestern Medical Center, Dallas under the guidance of Dr. Jefferey Cadeddu. Dr. Cadeddu is a renowned surgeon for carrying out laparoscopic surgeries on kidney and prostate. All the measurements were taken in accordance with the guidelines set by the Institutional Review Board of University of Texas at Arlington & the University of Texas Southwestern Medical Center Dallas.

The total number of patients analyzed for Kidney cancer was 23. Out of this, there were 12 cases of Radical Nephrectomy and 8 cases of Partial Nephrectomy. Three cases had to be neglected after the histology reported them to be Transitional cell Carcinoma, Hemorrhage Cyst and Papillary.

In the case of Prostate cancer the total number patients on whom the readings were recorded were 23. One case had to be neglected as the histologist did not receive any slides of the sample.

4.1 Experimental Protocol

The specimens are taken from the patients and then the frozen specimens were brought to the pathology room which was located outside the Operation Room. Firstly, the tumor size was measured and noted. The data was initially acquired by Ms. Disha Peswani and me. Later on, the data acquisition was done by Dr. Karim Bensalah and Dr. Altug Tuncel. They both were Urologists and were visiting scholars with Dr. Cadeddu. The setup for the experiment was explained in the earlier chapter.

The following were the steps of procedure:

1. Background light was recorded initially with the room lights and the light source switched off.
2. The probe was initially placed on the outer side of the sample and the reflectance spectra were acquired.
3. There was a reference chart prepared by the surgeons as to the exact locations on which the probe should be placed from the outside and from the inside. These locations were selected on the expertise of the maximum chances of occurrence of cancer. The maps are explained in detail in the following chapter.
4. After the outside readings were complete, dye was applied on the sample. Two separate dyes were applied on the either side of the sample, so that the exact section can be recognized after bi-halving the sample and for the histology.
5. The sample was then bi halved and the optical readings were recorded from the inside as per the reference map.
6. Also, after the readings were obtained at each location, that location was marked with a dye, so that the histologist will know the exact positioning of the probe.
7. After taking all the readings the sample was pinned up to a cardboard and then inserted in formaldehyde for preserving the sample for pathology

4.2 Kidney Data Analysis

As we know, in radical nephrectomy the entire kidney has to be removed. Figure 4.1 shows radical nephrectomy specimen. The schematic diagram for the placement of the probe to acquire the readings is shown in Fig 4.1.

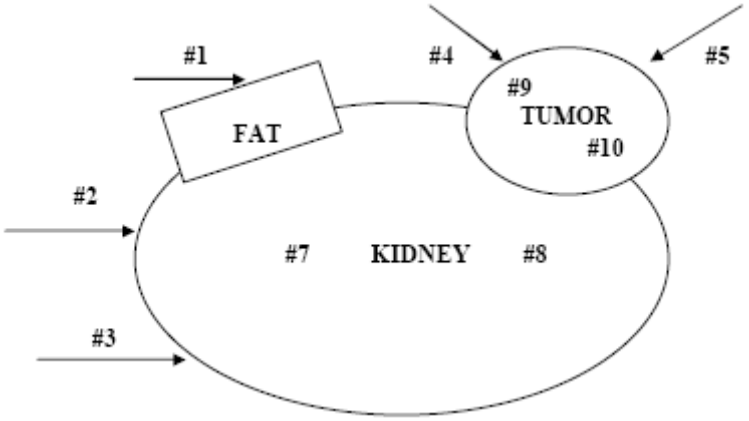

Figure 4.1: The above figure shows the schematic map for acquiring the spectrums in a radical nephrectomy.

The measurement #1 was taken on the surrounding perirenal fat. #2 & #3 were taken on the normal capsule of the kidney. The Tumor surface measurements were taken as #4 & #5. After the readings were taken from the outside the kidney was bi-halved. Another set of Normal Parenchyma (#7 & #8) were taken. The probe was placed in the tumor readings #9 & #10 were obtained. Thus for each patient there were a total of 10 locations on which the readings were taken.

The data points were then processed using the reflectance model and the optimization code. For analyzing the data, we included only 8 locations out of the total 10. The two locations omitted were the #1 Perirenal Fat & #6 surrounding fat. As the total number of patients was 12, therefore the total number of data points for analysis was 96. About 25 data points had to be omitted due to spectrum saturations, fitting mismatches and out-liners. Thus, the number of points used to classify the data was 71.

For obtaining readings from the partial nephrecotmy also, we had a reference schematic diagram, respective to which the probe was placed.

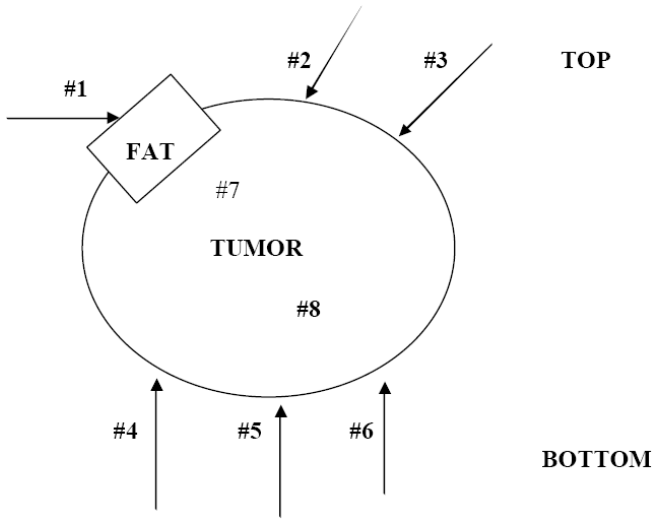

Figure 4.2: The above figure shows the schematic map for acquiring the spectrums in a partial nephrectomy.

#1 represents the peirenal fat on which the first reading was taken. Two readings were obtained on the capsule of the tumor (#2 & #3). The most interesting aspect about partial nephrectomy is the #5 location. This location is extremely critical for differentiation for the surgeon. The main reason being that, this point reflects the positive margin i.e. incase this point is tested as a cancer then there is a presence of a positive margin. The surgeon might need to make a further incursion to make sure that no cancerous tissue is left inside. #4 & #6 are the outer normal capsule readings. After bi-halving the sample, #7 & #8 were taken from inside the tumor. The total number of probe locations per subject was 8. Out of this only 6 locations were taken for analysis. #1 & #5 were omitted as they resembled the perirenal fat and a possible positive margin respectively. As the total number of patients was 8, thus the total number of data points analyzed was 48. Out of this 48 about 13 points had to be omitted during to spectrum saturation, mismatched fitting and out liners. Thus the number of points taken for analysis was 35.

The data was split into different categories depending upon the location and the tissue type. The initial classification was done between the readings taken on the outside for both

Radical and Partial combined together. The groups which were similarly classified were combined together so that we could improve the sample size and thus chance of getting a better statistical result. The two major comparisons were between then outside readings (control and tumor) & inside readings (control & tumor). The combined classification groups were as follows:

	Radical Nephrectomy Locations	Partical Nephrectomy Locations
Outside Control	#2 & #3	#4 & #6
Outside Tumor	#4 & #5	#2 & #3
Inside Control	#7 & #8	
Inside Tumor	#9 & #10	#7 & #8

Table 4.1: The above table shows the classification groups after combining both Radical and Partial together. The outside and the inside readings have been combined.

Physiologically, the Outside Tumor for Radical and Partial should have the same characteristics. Due to this fact both the cases have been combined. The spectrum characteristics obtained from the both the nephrectomies should ideally be the same. The below plots compare the oxy, deoxy hemoglobin and the scattering coefficient.

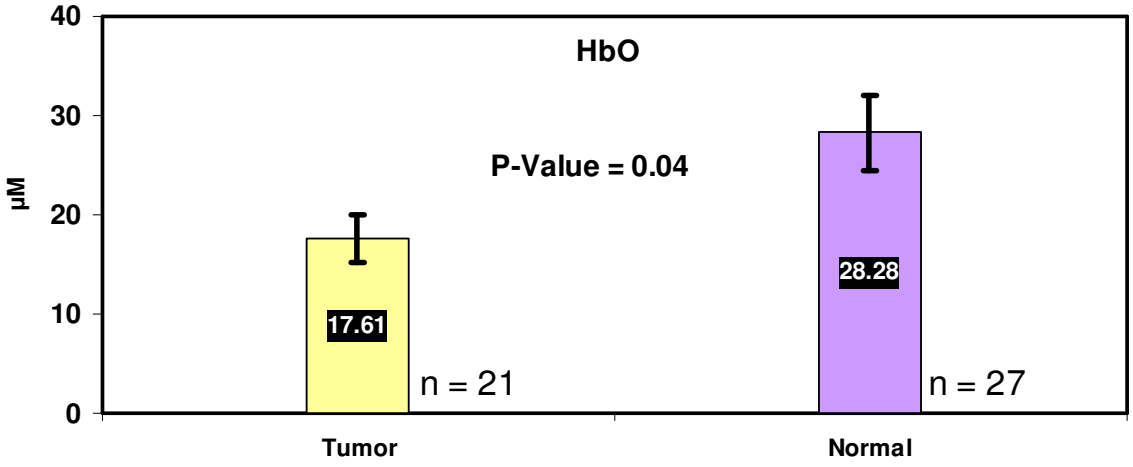

Figure 4.3: The above table shows the comparison for HbO for the outer readings of Radical and Partial Nephrectomy.

The student t-test was performed to check for any statistical difference between the categories. It is usually performed between two groups of means and if the final value is <0.05 then it is proved that those two categories are significantly different. If the P-Value is >0.05, they are said to have no differences.

In the above case, the oxy-hemoglobin is significantly higher in the control as compared to the cancerous tissue.

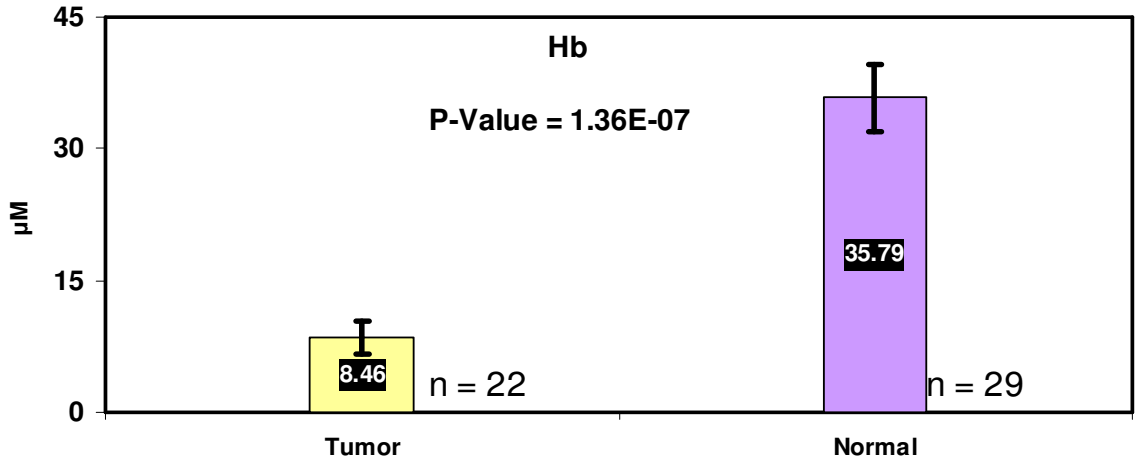

Figure 4.4: The above table shows the comparison for Hb for the outer readings of Radical and Partial Nephrectomy.

The graph above shows the difference in the deoxy hemoglobin [Hb]. We can observe that there is a significant difference in the outer parenchyma compared to the outer tumor capsule levels. This difference is clinically more important as the setup gives us the difference from the outside, which is more viable to the surgeon. From the graph below, the reduced scattering coefficient also gives us a statistical difference from the outside of the control and tumor.

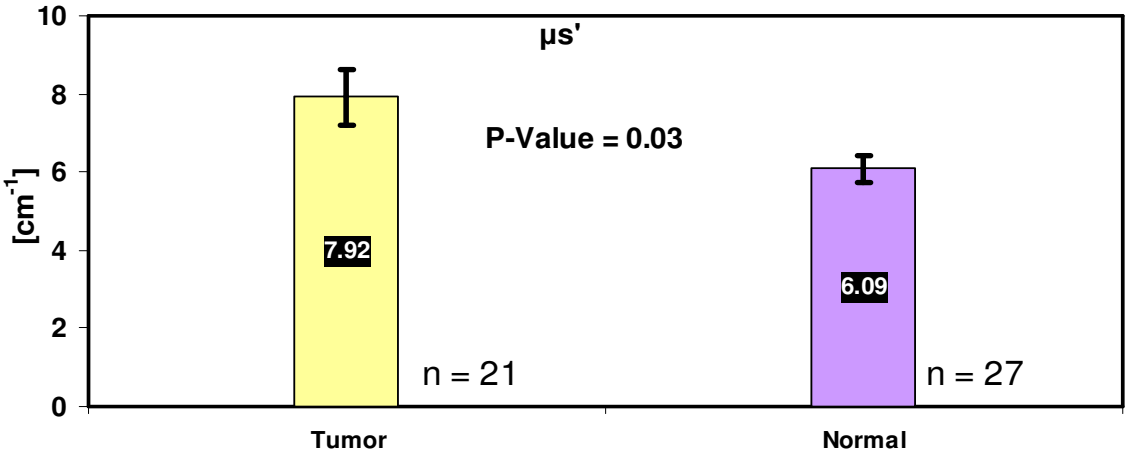

Figure 4.5: The above table shows the comparison for $\mu_{s'}$ between the different groups for radical nephrectomy.

These two conclusions can be a critical parameter for the clinical implementation of the setup. Thus the above results clearly signify that, there is a clear statistical difference between the control and the tumor. The oxygenation in the Normal tissues was significantly more than that of the cancer. Also, the reduced scattering coefficient for the tumor was more compared to that of the control. This could be correlated to the dense vasculature present in the tumor compared to that of normal. As the sample size is much larger than classifying them separately, the results are more validated. Similar comparison was done for the data obtained after bi-halving the sample. The P-Value was less than 0.05 for HbO and Hb, thus proving that the system can differentiate them statistically.

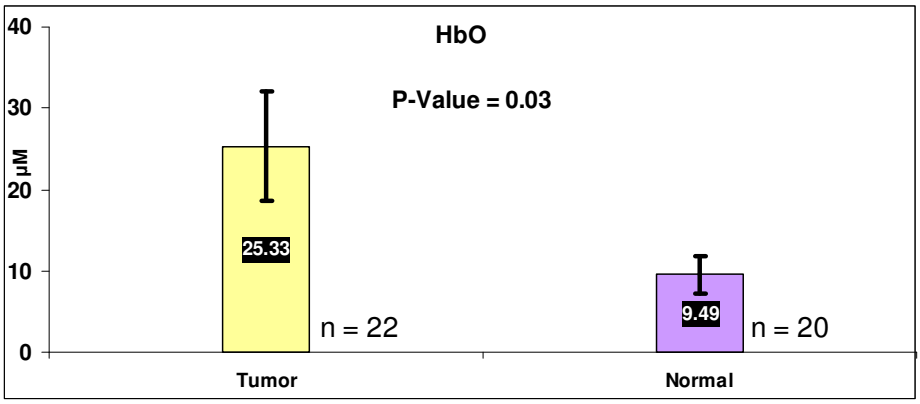

(A)

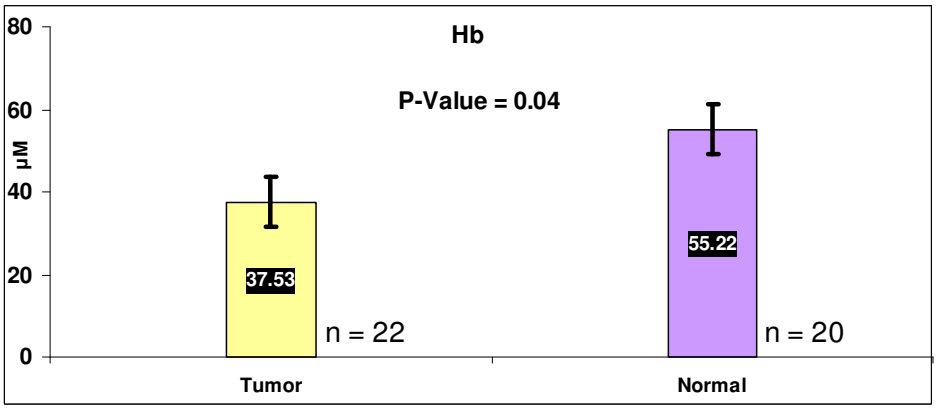

(B)

Figure 4.6: The above graphs depict the differentiation between the Tumor and the Normal regions from the inside.

It can be clearly seen that there is a significant difference in the oxygenation levels from the inside of the tissues too. The HbO is higher in the tumor than in the normal tissues after bi-halving.

To check the viability of the probe for detection of the positive margin an inverse calculation was conducted. In this case #4 & #6 locations were grouped together. They were classified as Control. This group was then compared to the values obtained for #5. In the entire sample of 23 patients, there was only one case of positive margin. While comparing these two, the #5 locations which were clubbed together were histologically control. Thus, after classification there should not be any significant difference between the two categories as they were both controls. If the system to indentify that, then there was definitely a scope for this

technique to be useful for detecting positive margins. The comparison was done for all the three parameters.

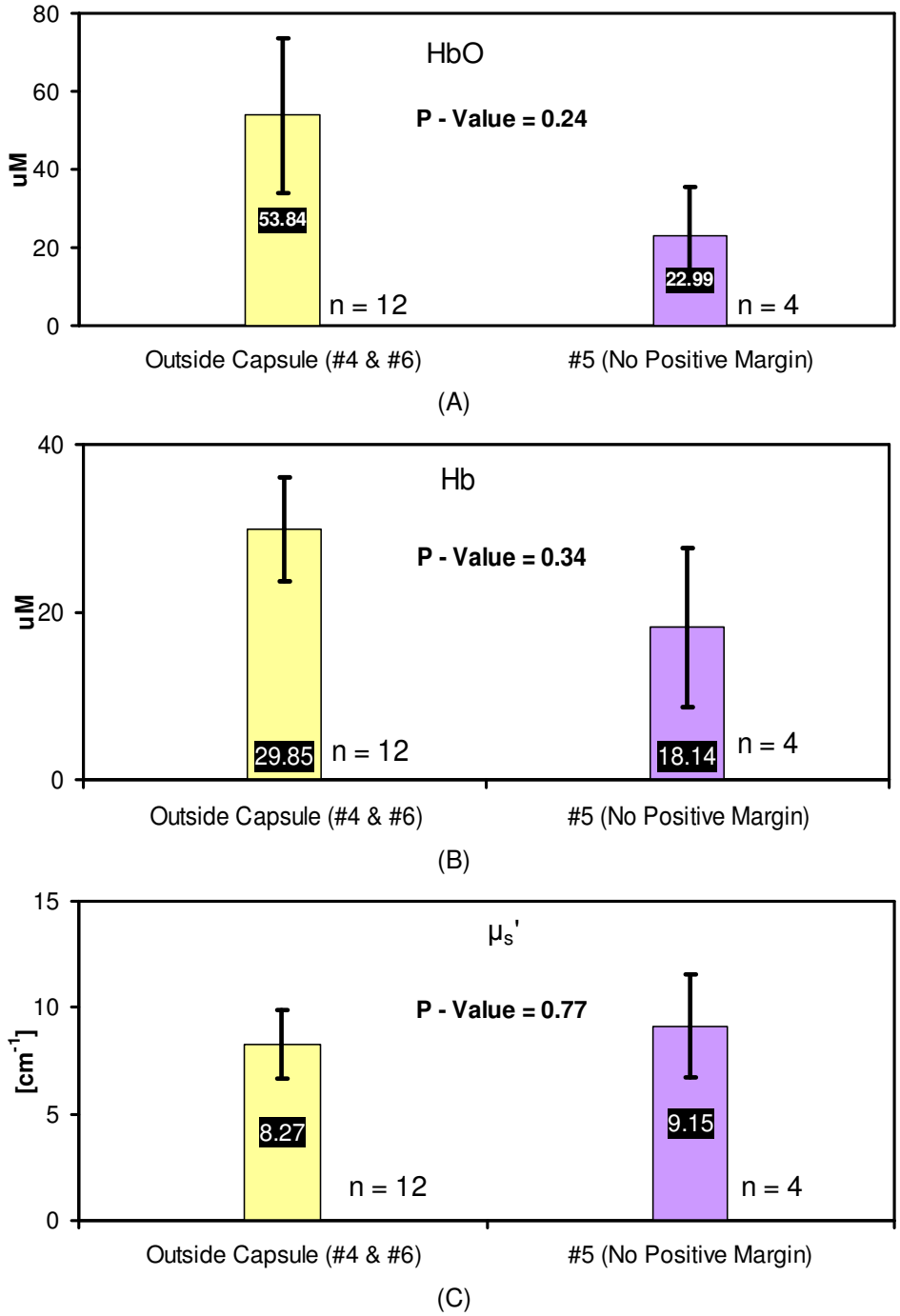

Figure 4.7: The graphs show the comparison between (A) HbO, (B) Hb and (C) μ_s' for viable detection of positive margin.

Thus it can be observed that none of the p-values are significant. This result increases the prospect of positive cancer detection.

Benign vs. Malignant Comparison

Initially the study was aimed at differentiating between the normal and the cancerous tissue. After the pathological analysis, the data was also classified as benign and malignant depending on the tissue type. In all there were about 29 data points for malignant and about 21 points for benign over the 20 patients which were analyzed. All the data points for malignant and benign were combined respectively irrespective of the kind of surgery (Radical or Partial).

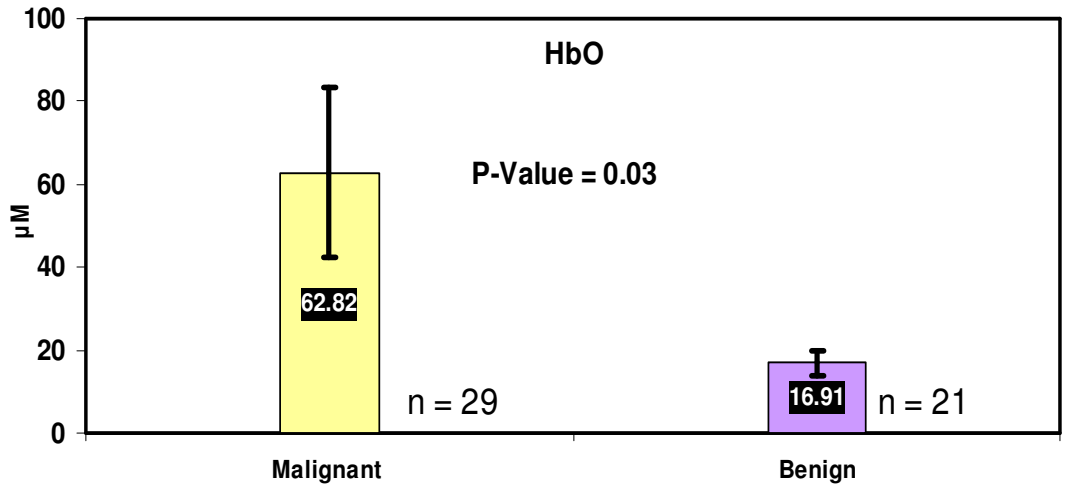

(A)

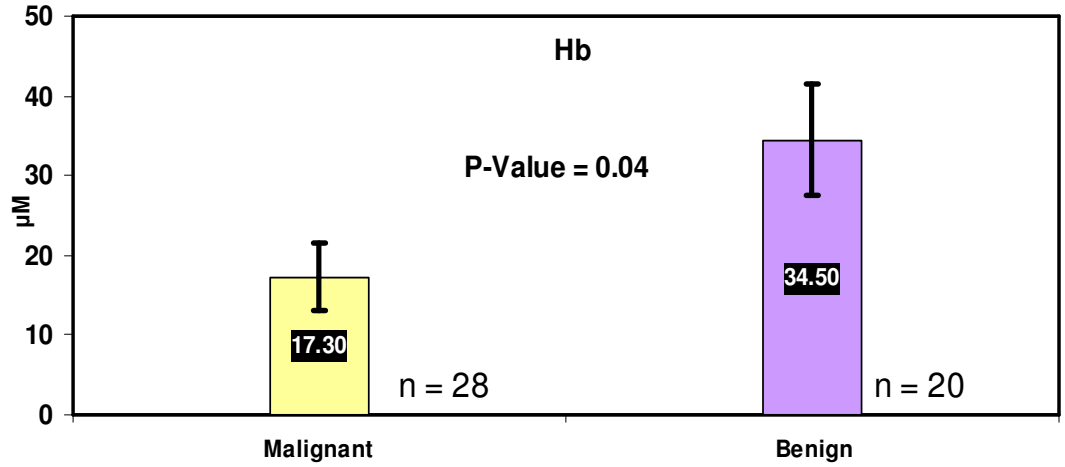

(B)

Figure 4.8: The above graphs show us the differentiation between the HbO(A) and Hb(B) for Benign & Malignant

From the above graph it can be clearly seen that there is a definite oxygenation change between the malignant and the benign. The oxy hemoglobin is higher in the malignant tissues compared to the benign tissues. Thus our tool is able to even differentiate the between malignant and benign tumors.

Prostate Analysis

In prostate cancer analysis, the entire prostate gland along with the seminal vesicles is taken out. The locations for acquiring the data are taken from a schematic map shown in the following figure. Total of 16 readings were taken on each prostate sample. Out of them, 6 were taken from the outside and the rest were taken after bi halving the sample.

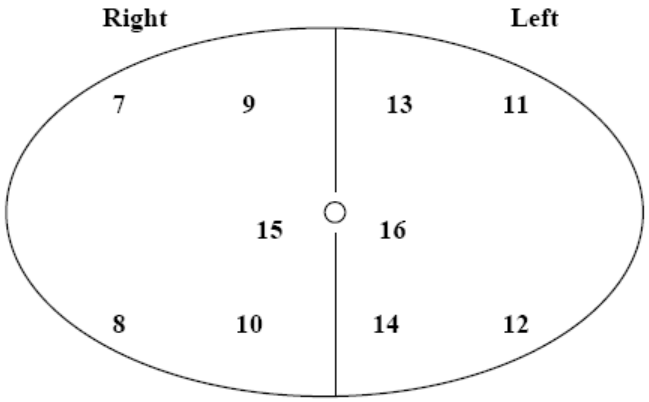

Figure 4.9: The figure shows the locations on which the spectrums were obtained after bi halving the sample.

Readings #1 & #2 were taken on the apex from the outside of the prostate. #3 & #4 were taken on the Neurovascular bundle and #5 & #6 were obtained on the outer capsule of the prostate. In the above figure #7, 8,9,10 resemble the right peripheral zone & #11, 12, 13, 14 resemble the left peripheral zone. #15 & #16 are the transitional zone readings. For prostate we had a total of 23 patients. The total number of data points analyzed was 9 for each patient. Thus the total number of points analyzed for classification was 202. The data was classified as Tumor and Control based on the pathological analysis.

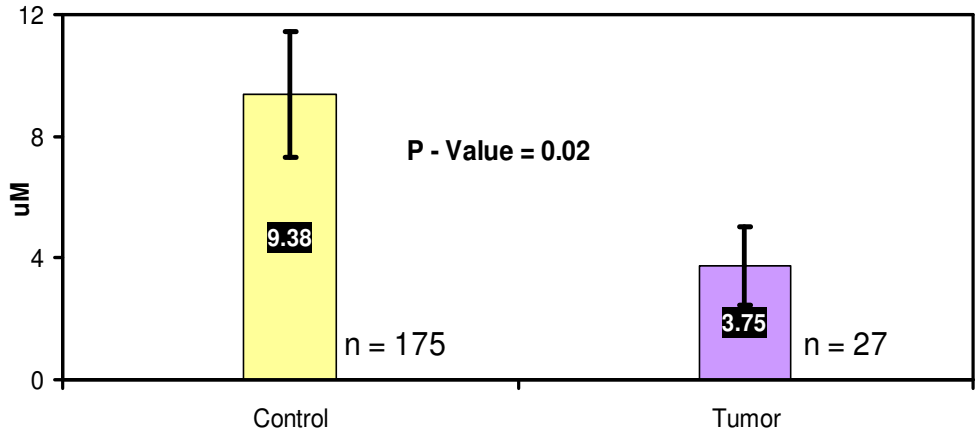

(A)

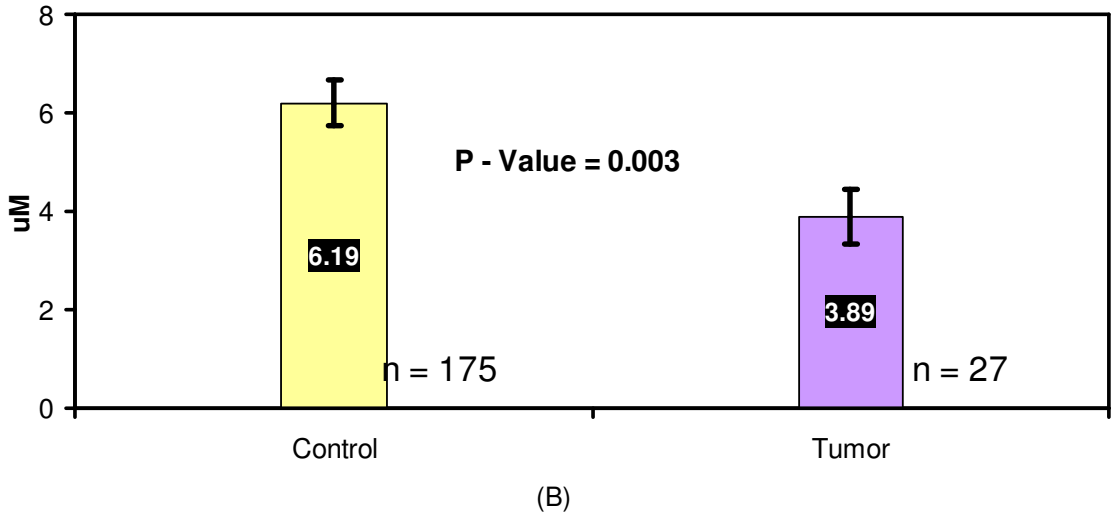

(B)

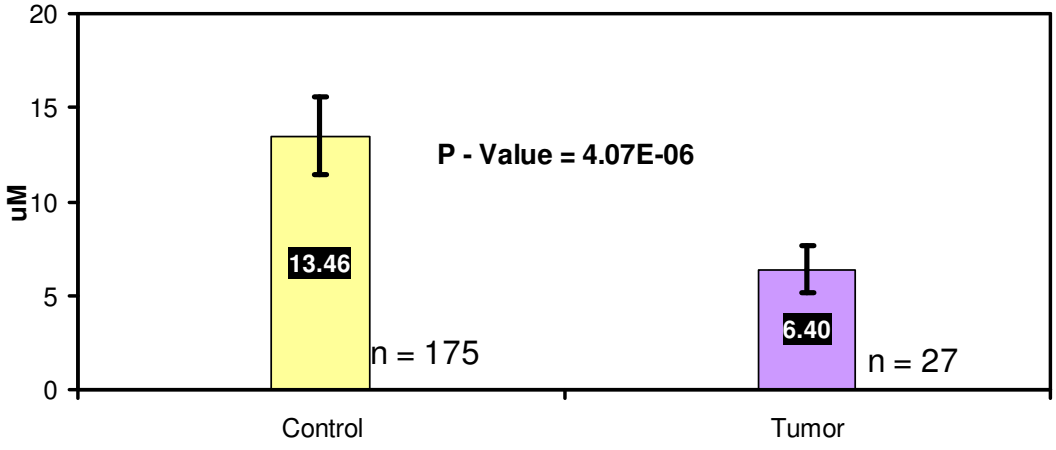

(C)

Figure 4.10: The above graphs depict the differentiation between the normal and tumor tissues for HbO, Hb & HbT.

As observed, the data was processed and the concentrations of blood oxygenation levels were obtained. There were a total of 175 readings for control and 27 for cancer. We can see that there is a significant difference in the levels of oxy hemoglobin between normal and cancer. The P-Value of 0.003 also justifies the fact that our setup has the capability to differentiate between the normal and the tumor on basis of de oxy hemoglobin. The total blood concentration is also higher in the control as compared to the tumor. For further analysis, the data was also classified and compared with the outer readings. The results are shown below.

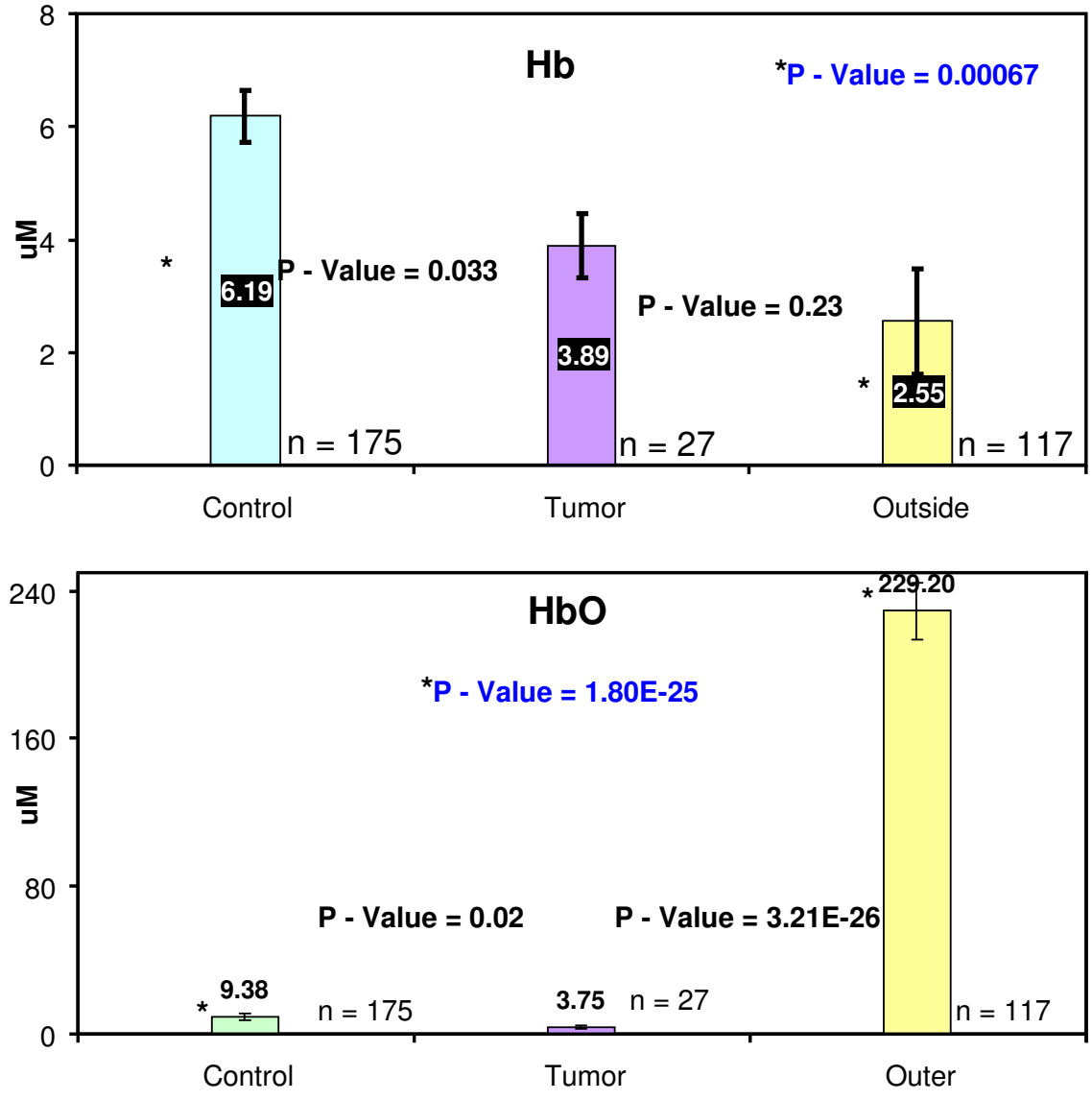

Figure 4.11: The graphs show the comparison between the inner readings and the outer readings for prostate.

The oxy hemoglobin level for the outer capsule readings was significantly higher as compared to that of the inner locations. This significance adds to the feasibility of the technique to be implemented on the outside of the prostate to differentiate between the normal the cancer.

CHAPTER 5

DISCUSSION AND FUTURE SCOPE

Reflectance Spectroscopy has been a recognized as a viable tool for understanding the tissue characteristics. This technique has been used in detection of cancer in ovaries, breasts and also the cervical.

The main aim of this study was to differentiate between the normal and the tumor tissues in both prostate and the kidney. The theory of diffuse reflectance could not be implemented in this case as the source detector separation was very small. Thus, the spectrums were analyzed using the published reflectance model. The main pre requisite of the model is the detection of the k1 & k2 values. Rigorous calibrations were done to understand the dependence and the characteristic of these parameters and their effect on the setup used.

After the model was formulated, the classification poised as a challenge due to the various categories involved. Most of the classification was done based on the clinical requirements of the surgeon. We were able to differentiation the normal and tumor tissues in kidney from the outside as well as from the inside based on the blood oxygenations and also the light scatterings. Our technique could be a viable tool for the detection of positive margin in partial nephrectomies and also for the differentiation between malignant and benign. The higher oxygenation level in the malignant tissue could be attributed to the fact that the cells in malignant tumor are more active and they multiple in a uncontrolled manner [16].

For the prostate cancer, we could statistically differentiate the normal and the tumor tissues. This is a significant milestone considering the complex structure of the prostate tissues and also the varied locations of the tumors. To further quantify the results obtained from the code we intend to implement classification algorithms using the leave one out analysis which

could give us a more rigorous way to differentiate between the normal and the cancerous tissues.

REFERENCES

1. Website of Wikipedia: http://en.wikipedia.org

2. Website of Cancer Help : http://www.cancerhelp.org.uk/help/default.asp?page=4048# radical

3. Website of Biomedical Optics Research Laboratory http://www.medphys.ucl.ac.uk/research/borl/research/NIR_topics/nirs.htm

4. Website of Prostate Cancer : www.prostatecancercentre.co.uk/theprostate.html

5. Website of Wikipedia : http://en.wikipedia.org/wiki/Prostate

6. M. Johns, C. Giller, D. German, and H. Liu, "Determination of reduced scattering coefficient of biological tissue from a needle-like probe," Opt. Express **13**, 4828-4842 (2005)

7. Website of Wikipedia : http://en.wikipedia.org/wiki/Near_infrared_spectroscopy

Krahn, MD; Mahoney JE, Eckman MH, Trachtenberg J, Pauker SG, Detsky AS (Sep 14 1994). "Screening for prostate cancer.. A decision analytic view". JAMA 272 (10): 773-80.

8. Website of Prostate Cancer : www.prostatecancercentre.co.uk/theprostate.html

9. Website of Prostate Cancer : http://www.pueblo.gsa.gov/cic_text/health/prostate/prostate.html

10. Website of Ocean Optics : http://oceanoptics.com/

11. Website of General Information about Prostate Cancer : www.meb.uni-bonn.de/cancer.gov/CDR0000062965.html

12. Website of Wikipedia : http://en.wikipedia.org/wiki/Prostate

13. Website of Washington State University for Near Infra Red Spectroscopy:

14. Website of Patient Health: http://www.patienthealthinternational.com

15. Website of Healing Daily. http://healingdaily.com

16. H. Liu, Y. Gu, J. G. Kim, and R. P. Mason, "Near-Infrared Spectroscopy and Imaging of Tumor Vascular Oxygenation," *Methods in Enzymology*, vol. 386, pp. 349-378, 2004.

17. G. Zonios and A. Dimou, "Modeling diffuse reflectance from semi-infinite turbid media: application to the study of skin optical properties," *Optics Express*, vol. 14, pp. 8661-8674, 2006.

18. M. Dorigo, V. Maniezzo, and A. Colorni, "Ant System: Optimization by a colony of cooperating agents," *IEEE Transactions on Systems, Man, and Cybernetics-Part B*, vol. 26, pp. 29-41, 1996.

19. M. Johns, C. A. Giller, D. German, and H. Liu, "Determination of reduced scattering coefficient of biological tissue from a needle-like probe," *Optics Express*, vol. 13, pp. 4828-4842, 2005.

20. S. T. Flock, S. L. Jacques, B. C. Wilson, W. M. Star, and M. J. C. Van Gemert, "Optical properties of intralipid: A phantom medium for light propagation studies," *Lasers in Surgery and Medicine*, vol. 12, pp. 510-519, 1992.

21. H. J. Van Staveren, C. J. M. Moes, J. v. Marle, S. A. Prahl, and M. J. C. Van Gemert, "Light scattering in Intralipid-10% in the wavelength range of 400-1100 nm," *Applied Optics*, vol. 30, pp. 4507-4514, 1991.

22. Kashyap D. “Development Of A Broadband Multi-Channel Nirs System For Quantifying Absolute Concentrations Of Hemoglobin Derivatives And Reduced Scattering Coefficients”. Doctoral Dissertation, University of Texas at Arlington 2007.

BIOGRAPHICAL INFORMATION

Aditya Vivek Mathker was born on December 26th, 1983 in Mumbai, India. He received his Bachelor of Engineering degree in Biomedical Engineering from Mumbai University, India in June 2006. During this tenure he did six months internship at Jaslok hospital and Research Center at Mumbai as a Biomedical Engineer Trainee.

In fall 2006 he started his graduate studies in Biomedical Engineering from the Joint program of Biomedical Engineering at the University of Texas at Arlington and University of Texas at Southwestern Medical Center at Dallas completing it summer 2008. His research interests include Medical device development and formulating fault finding algorithms for medical equipments.